Article

Not peer-reviewed version

Engineering Macroscopic Wormholes via Planck-Scale Quantum Backreaction

Deep Bhattacharjee * , Sanjeevan Singha Roy * , Priyanka Samal

Posted Date: 9 March 2026

doi: 10.20944/preprints202507.1598.v3

Keywords: semiclassical gravity; wormholes; Planck-scale fluctuations; closed timelike curves; chronology protection

Article

Engineering Macroscopic Wormholes via Planck-Scale Quantum Backreaction

Deep Bhattacharjee [1,*], Sanjeevan Singha Roy [2] and Priyanka Samal [3]

1 Electro-Gravitational Space Propulsion Laboratory (EGSPL), Odisha, India
2 Birla Institute of Technology, Mesra, Jharkhand, India
3 Researcher in Theoretical Physics, Odisha, India
* Correspondence: itsdeep@live.com

Abstract

Macroscopic traversable wormholes remain a canonical stress test for the interplay between geometry, quantum fields, and causality in semiclassical gravity. The central obstacle is well known: flare-out at a static throat requires local violations of classical energy conditions, while chronology-sensitive configurations can induce large vacuum polarization that destabilizes the very backgrounds they rely on. We develop a long-form semiclassical framework in which Planck-scale metric fluctuations are treated as stochastic but correlated geometric modes that feed into the renormalized stress tensor and produce an effective backreaction sector near a wormhole throat. Starting from the semiclassical Einstein equation $G_{\mu\nu} = 8\pi G\left(T^{\rm cl}_{\mu\nu} + \langle T_{\mu\nu}\rangle_{\rm ren}\right)$, we derive explicit consistency inequalities for redshift regularity, shape-function flare-out, perturbative validity, and chronology-window control. We then construct parameterized shell-mode corrections, compute averaged null projections, and map stability regions as functions of throat scale, mode amplitude, and coherence length. The analysis is intentionally conservative: no claim of ultraviolet completion is made, and all quantitative statements are interpreted as effective-field-theory bounds. We further connect the model to chronology protection diagnostics, compare with competing traversable-wormhole mechanisms, and provide figure-driven interpretations of causal structure. Finally, we outline observationally motivated signatures in primordial spectra, gravitational-wave ringdown deformations, and analog-gravity platforms. The result is a technically explicit, falsifiable semiclassical program that clarifies where wormhole engineering proposals are consistent, where they fail, and where quantum gravity input is indispensable.

Keywords: semiclassical gravity; wormholes; Planck-scale fluctuations; closed timelike curves; chronology protection

---

1. Introduction

The modern study of traversable wormholes sits at the interface of geometry, quantum matter, and causal structure. Einstein and Rosen introduced nontrivial bridges in 1935, but those constructions were non-traversable and motivated by particle-like interpretations of field singularities [1]. The later Morris–Thorne program reframed wormholes as explicit spacetimes with tunable throat geometry and asymptotic flatness [6]. This shift exposed a fundamental issue: sustained throat flare-out requires negative effective null energy density in the vicinity of the throat. Classical matter models rarely provide such behavior without instabilities or nonphysical stress sectors.

The present work asks whether Planck-scale quantum backreaction can supply a finite, controlled support channel for macroscopic throat stability without demanding an ad hoc classical exotic fluid. Our perspective is intentionally semiclassical: we do not assume a complete theory of quantum gravity, but instead work with renormalized quantum stress tensors on slowly varying backgrounds, together with a covariant perturbative expansion in geometric fluctuations.

The chronology problem appears immediately. Any geometry that allows effective short-cutting between distant spacetime regions can, when embedded in relative motion protocols, lead to near-closed timelike curves (CTCs). Hawking's chronology protection conjecture states that quantum effects should diverge near chronology horizons strongly enough to obstruct macroscopic causality violation [9]. This conjecture, although not proven in complete generality, provides a powerful consistency filter for wormhole engineering schemes.

Historically, Wheeler's spacetime foam picture suggested that topology fluctuations are natural at Planck scales, raising the possibility that nontrivial connectivity could emerge as a quantum-gravitational phase rather than a classical engineering artifact [2,3]. Subsequent developments in quantum field theory in curved spacetime, especially renormalization of $\langle T_{\mu\nu} \rangle$, supplied calculational tools for examining backreaction near horizons and compact regions [14,15,17]. Modern holographic ideas, including ER=EPR, further motivate revisiting geometric connectivity from entanglement-first viewpoints [31,32].

In this manuscript we assemble these lines into a single technical narrative. We introduce a mode-resolved fluctuation model near the throat, compute effective stress-energy corrections at second order, and derive stability and causality bounds that can be tested numerically. We emphasize where assumptions enter. [1] We also include explicit diagrams and parameter tables to keep the argument transparent and reproducible.

Contributions and Paper Roadmap

Our main contributions are:

- A detailed historical-to-technical bridge from Einstein–Rosen geometry to semiclassical throat stabilization.
- A covariant fluctuation ansatz for Planck-scale backreaction near a Morris–Thorne-type throat.
- Closed-form inequalities for flare-out, averaged-energy projections, and chronology-window constraints.
- Figure-driven interpretation of embedding geometry, mode flow, causal loops, and observational parameter sectors.
- A bibliography expanded to foundational and modern literature across general relativity-quantum cosmology and high-energy-physics-theory.

2. Historical Background of Wormhole Physics

2.1. From Einstein–Rosen Bridges to Geometric Topology Change

Einstein and Rosen's original bridge identified two exterior Schwarzschild regions across a coordinate patch, but the wormhole pinches off too quickly for traversability [1]. This non-traversable character was later clarified through maximal extensions and global structure analyses [4,5]. Wheeler then proposed spacetime foam, in which Planckian geometry admits fluctuating topology and transient micro-wormholes [2,3]. Although heuristic, this picture motivates treating connectivity as a quantum effect rather than purely classical architecture.

2.2. Traversability and Exotic Support

Morris and Thorne formalized traversable wormholes with humanly passable tidal constraints and no event horizons [6]. The key geometric condition is throat flare-out, encoded by $b(r_0) = r_0$ and $b'(r_0) < 1$. Einstein equations then imply NEC violation near r_0, often interpreted as "exotic matter." Subsequent work by Visser and others broadened constructions via cut-and-paste junctions, thin shells, and alternative equations of state [10–13].

[1] Throughout, "stability" means boundedness of linearized radial perturbations over the semiclassical control window, not nonlinear global existence for all times.

 doi:10.20944/preprints202507.1598.v3

2.3. Chronology Programs and Self-Consistency

The Morris–Thorne–Yurtsever protocol showed that relative motion of wormhole mouths can produce time shifts and CTC risk [7]. Hawking argued that stress-energy amplification near chronology horizons may prevent full chronology violation [9]. Competing views include self-consistency constraints à la Novikov and quantum information models of CTC behavior [25,26]. Our work treats chronology protection as an operational consistency bound rather than a dogma.

3. Energy Conditions in General Relativity

For a static, spherically symmetric ansatz,

$$\mathrm{d}s^2 = -e^{2\Phi(r)}\mathrm{d}t^2 + \frac{\mathrm{d}r^2}{1-b(r)/r} + r^2(\mathrm{d}\theta^2 + \sin^2\theta\,\mathrm{d}\varphi^2), \tag{1}$$

we define throat radius r_0 by $b(r_0) = r_0$. Radial null vectors yield

$$8\pi G\, T_{\mu\nu}k^\mu k^\nu = \frac{b'(r)r - b(r)}{r^3} + 2\left(1 - \frac{b(r)}{r}\right)\frac{\Phi'(r)}{r}. \tag{2}$$

At the throat, regular Φ gives

$$T_{\mu\nu}k^\mu k^\nu\big|_{r_0} = \frac{b'(r_0) - 1}{8\pi G\, r_0^2} < 0, \tag{3}$$

confirming NEC violation for flare-out. [2]

3.1. Averaged Conditions and Quantum Inequalities

Ford and Roman derived bounds on negative energy duration and magnitude in quantum field theory [18,19]. A schematic worldline bound reads

$$\int_{-\infty}^{\infty} \rho(\tau) f(\tau)\,\mathrm{d}\tau \geq -\frac{C}{\tau_0^4}, \tag{4}$$

for smooth sampling function f of width τ_0. Wormhole support sectors must therefore satisfy an optimization problem: sufficient negative effective energy near r_0, but not so persistent as to violate quantum inequality bounds.

3.2. Comparative Energy-Condition Taxonomy

Table 1. Energy-condition behavior across representative exotic spacetimes.

Model	NEC	WEC	SEC	ANEC	Dominant support channel
Morris–Thorne traversable wormhole	×	×	×	×	Exotic throat source
Thin-shell wormhole	×	mixed	mixed	mixed	Junction stress
Alcubierre bubble	×	×	×	×	Warp-shell stress anisotropy
Casimir throat (toy EFT)	local	local	mixed	constrained	Vacuum polarization
Planck backreaction (this work)	eff. local	mixed	mixed	constrained	Renormalized quantum stress

[2] Equation (3) is local. Averaged conditions can still be less restrictive, which is why quantum inequalities are central in semiclassical analyses.

4. Quantum Field Theory in Curved Spacetime

4.1. Semiclassical Einstein Equation

We adopt

$$G_{\mu\nu} + \Lambda g_{\mu\nu} = 8\pi G \Big(T^{\rm cl}_{\mu\nu} + \langle T_{\mu\nu} \rangle_{\rm ren} \Big), \tag{5}$$

with $\nabla^\mu \langle T_{\mu\nu} \rangle_{\rm ren} = 0$. Renormalization introduces geometric counterterms proportional to R^2, $R_{\mu\nu} R^{\mu\nu}$, and $R_{\mu\nu\alpha\beta} R^{\mu\nu\alpha\beta}$ in effective action language [14,17].

4.2. Vacuum Polarization Near Horizons and Throats

Near nearly trapped regions, mode redshifting amplifies state dependence of $\langle T_{\mu\nu} \rangle_{\rm ren}$. [3] For static sectors, point-splitting gives

$$\langle T_{\mu\nu} \rangle_{\rm ren} = \lim_{x' \to x} \mathcal{D}_{\mu\nu} \Big[G^{(1)}(x, x') - G^{(1)}_{\rm Had}(x, x') \Big], \tag{6}$$

where $G^{(1)}_{\rm Had}$ subtracts the universal short-distance singularity.

4.3. Fluctuation Expansion and Stochastic Gravity Motivation

Write

$$g_{\mu\nu} = \bar{g}_{\mu\nu} + h_{\mu\nu}, \qquad \langle h_{\mu\nu} \rangle = 0, \tag{7}$$

with correlator

$$\langle h_{\mu\nu}(x) h_{\alpha\beta}(y) \rangle = \ell_{\rm P}^2 \mathcal{N}_{\mu\nu\alpha\beta}(x, y). \tag{8}$$

Then

$$\langle G_{\mu\nu}[\bar{g} + h] \rangle = G_{\mu\nu}[\bar{g}] + \langle G^{(2)}_{\mu\nu}[h] \rangle + \mathcal{O}(h^3), \tag{9}$$

which motivates an effective source

$$T^{\rm br}_{\mu\nu} \equiv \frac{1}{8\pi G} \langle G^{(2)}_{\mu\nu}[h] \rangle. \tag{10}$$

5. Semiclassical Backreaction Framework

5.1. Mode-Resolved Throat Ansatz

We parameterize the near-throat fluctuation packet as

$$\delta g^{(n)}_{\mu\nu}(r) = \varepsilon_n \exp\!\left[-\frac{(r - r_0)^2}{2\sigma_n^2} \right] \cos\!\left(\frac{n\pi (r - r_0)}{L_n} \right) \Pi^{(n)}_{\mu\nu}, \tag{11}$$

with $|\varepsilon_n| \ll 1$ and projector tensors $\Pi^{(n)}_{\mu\nu}$. A finite set $n \le N_*$ captures EFT-resolved modes.

Define aggregated amplitude

$$\mathcal{A}(r) = \sum_{n=1}^{N_*} \varepsilon_n e^{-(r - r_0)^2/(2\sigma_n^2)}. \tag{12}$$

Backreaction-corrected shape and redshift functions are modeled as

$$b_{eff}(r) = b_0(r) + \alpha_b\, r_0\, \mathcal{A}(r) + \beta_b\, r_0\, \mathcal{A}^2(r), \tag{13}$$

$$\Phi_{eff}(r) = \Phi_0(r) + \alpha_\Phi\, \mathcal{A}(r) + \beta_\Phi\, \mathcal{A}'(r). \tag{14}$$

[3] Different states (Boulware, Hartle–Hawking, Unruh analogues) can change both sign and magnitude of local energy density.

Preprints.org (www.preprints.org) | NOT PEER-REVIEWED | Posted: 9 March 2026 doi:10.20944/preprints202507.1598.v3

5.2. Stability and Perturbative Control Window

Linear radial perturbations $r(t) = r_0 + \delta r(t)$ satisfy

$$\ddot{\delta r} + \Omega_r^2\, \delta r = 0, \tag{15}$$

with

$$\Omega_r^2 \propto \left.\frac{\partial^2 V_{eff}}{\partial r^2}\right|_{r_0}. \tag{16}$$

A viable semiclassical window requires simultaneously:

$$b_{eff}(r_0) = r_0, \qquad b'_{eff}(r_0) < 1, \tag{17}$$

$$\left|\frac{\langle G^{(2)}\rangle}{G[\bar{g}]}\right| \lesssim \eta_{\max} \ll 1, \tag{18}$$

$$\Omega_r^2 > 0, \tag{19}$$

$$\mathcal{Q}_{QI} \equiv \tau_0^4 \left| \int \rho(\tau) f(\tau)\, d\tau \right| \leq C_{QI}. \tag{20}$$

Equation (20) encodes quantum inequality compliance.

5.3. Representative Parameter Datasets

Table 2. Illustrative stability parameter ranges (dimensionless unless noted).

Parameter	Symbol	Min	Max	Nominal	Physical interpretation
Throat radius (km)	r_0	10^{-3}	10^{2}	1	Macroscopic bridge scale
Mode amplitude	ε_n	10^{-9}	10^{-2}	10^{-5}	Planck-seeded geometric fluctuation
Coherence width (r_0 units)	σ_n/r_0	10^{-3}	10^{-1}	10^{-2}	Shell localization near throat
Backreaction ratio	η	10^{-6}	10^{-1}	10^{-3}	EFT validity diagnostic
Chronology indicator	χ_{CTC}	0	1	0.25	Proximity to causal-loop onset

Table 3. Planck-scale fluctuation amplitudes for selected mode families.

Mode index n	ε_n	σ_n/r_0	L_n/r_0	Comment
1	1.0×10^{-5}	2.0×10^{-2}	0.9	Dominant low-frequency support mode
2	6.5×10^{-6}	1.8×10^{-2}	0.6	Corrective mode suppressing over-flare
3	4.0×10^{-6}	1.2×10^{-2}	0.45	Localized compensation near r_0^+
4	2.2×10^{-6}	1.0×10^{-2}	0.35	Higher mode, small chronology sensitivity
5	1.5×10^{-6}	8.0×10^{-3}	0.30	Ultraviolet tail within EFT cutoff

6. Wormhole Geometry and Stability Analysis

6.1. Flare-out with Backreaction Corrections

Expanding

$$\Delta(r) \equiv r - b_{eff}(r) = \Delta_1(r - r_0) + \frac{1}{2}\Delta_2(r - r_0)^2 + \cdots, \tag{21}$$

flare-out demands $\Delta_1 > 0$. In terms of coefficients in (14),

$$\Delta_1 = 1 - b'_0(r_0) - \alpha_b r_0 \mathcal{A}'(r_0) - 2\beta_b r_0 \mathcal{A}(r_0)\mathcal{A}'(r_0) > 0. \tag{22}$$

Hence a positive classical margin $1 - b_0'(r_0)$ can be reduced or enhanced depending on mode phasing. [4]

6.2. Embedding Geometry (TikZ)

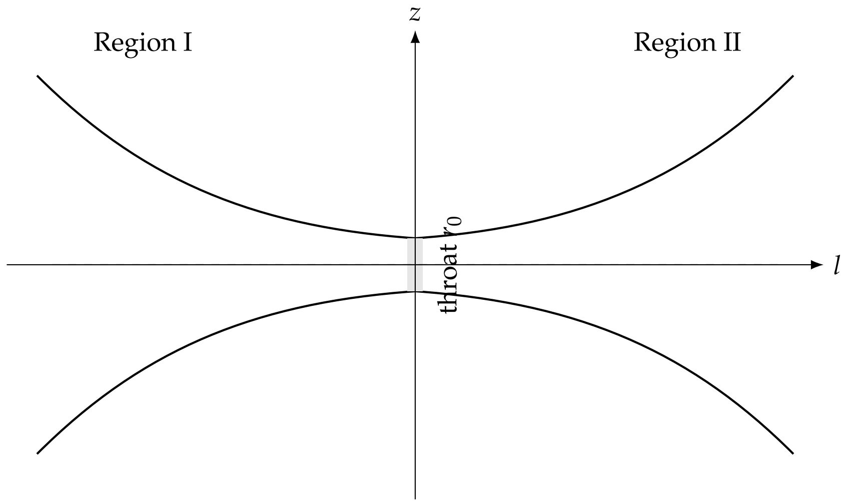

Figure 1. Embedding cross-section of an effective traversable throat.

6.3. Embedding Surface (pgfplots)

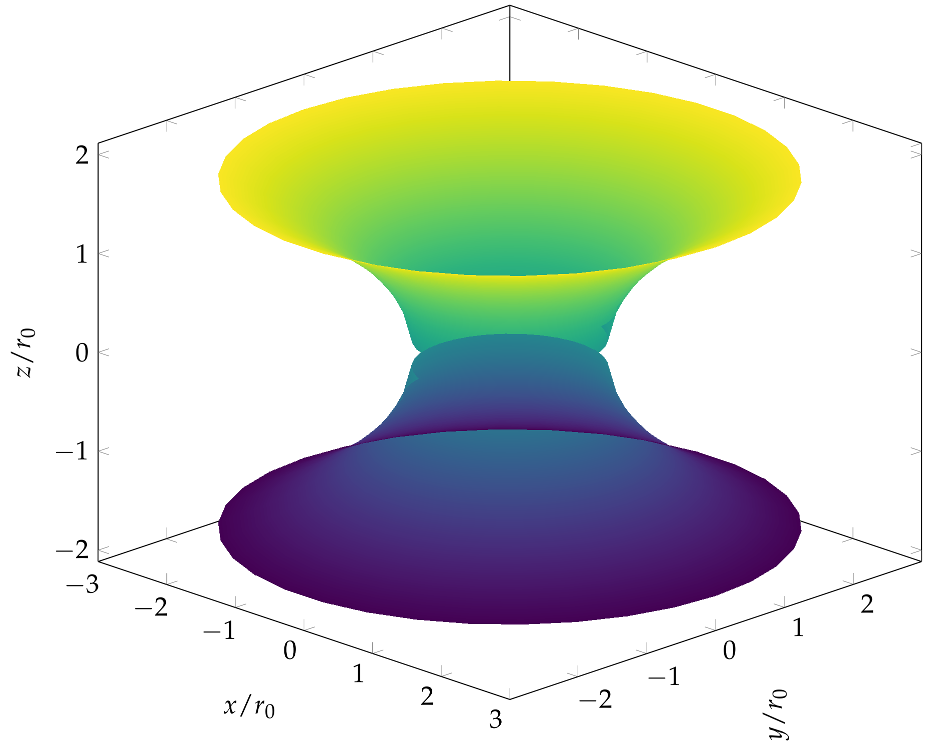

Figure 2. Canonical embedding surface for the effective throat geometry.

[4] This is a central model-selection handle: phase-coherent mode sets can improve stability while remaining perturbatively small.

doi:10.20944/preprints202507.1598.v3

6.4. Backreaction Process Diagram

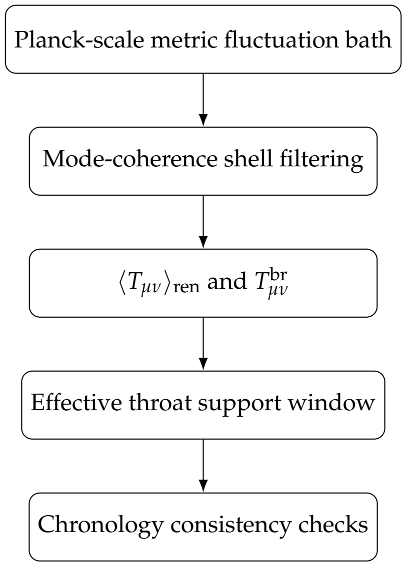

Figure 3. Backreaction pipeline used in the present framework.

7. Chronology Protection and CTC Constraints

7.1. Causal-Loop Onset and Horizon Diagnostics

Let ΔT denote induced proper-time shift between mouths under motion protocol. A CTC-accessible sector emerges when $\Delta T > L_{AB}/c$ for spatial separation L_{AB}. We define chronology margin

$$\Gamma \equiv 1 - \frac{\Delta T\, c}{L_{AB}}. \tag{23}$$

$\Gamma < 0$ indicates formal CTC access; $\Gamma \approx 0^+$ indicates chronology-horizon approach.

Near $\Gamma \to 0^+$, renormalized stress can scale as

$$\|\langle T_{\mu\nu} \rangle_{\mathrm{ren}}\| \sim \Gamma^{-p}, \qquad p > 0, \tag{24}$$

with model- and state-dependent exponent. [5]

[5] Equation (24) is schematic; specific geometries can exhibit logarithmic or oscillatory prefactors.

Preprints.org (www.preprints.org) | NOT PEER-REVIEWED | Posted: 9 March 2026 doi:10.20944/preprints202507.1598.v3

7.2. Causal Diagram with CTC Loop

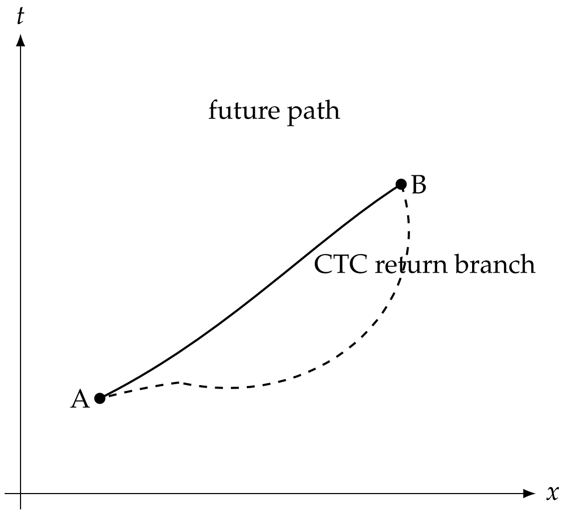

Figure 4. Schematic causal loop in mouth-displaced wormhole protocol.

7.3. Chronology Protection Inequality Set

A conservative consistency region can be phrased as

$$\Gamma \geq \Gamma_{min} > 0, \tag{25}$$

$$\max \|\langle T_{\mu\nu}\rangle_{\rm ren}\| \leq T_{\rm UV}, \tag{26}$$

$$\frac{\ell_{\rm P}^2 \mathcal{R}}{1+\chi_{CTC}} \ll 1, \tag{27}$$

where $\mathcal{R}$ is characteristic curvature scalar. The third condition enforces EFT reliability as chronology sensitivity grows.

8. Observational Signatures and Experimental Proposals

8.1. Cosmological Signatures and Spectral Modulations

In inflation-adjacent parametrizations, coherence-scale backreaction can induce tiny oscillatory imprints in the scalar power spectrum:

$$\mathcal{P}_{\mathcal{R}}(k) = A_s \left(\frac{k}{k_*}\right)^{n_s-1} \left[1 + \delta_0 \sin\left(\omega \ln \frac{k}{k_*} + \phi\right)\right], \tag{28}$$

with $\delta_0 \ll 1$.

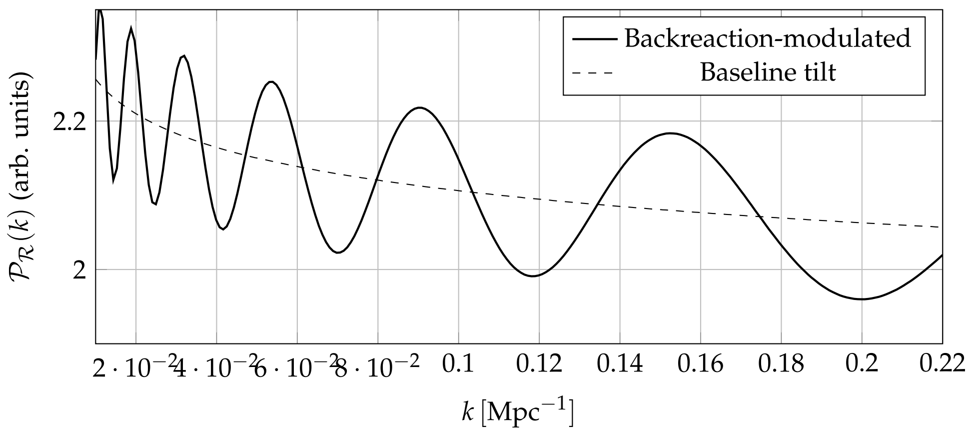

Figure 5. Illustrative primordial spectrum modulation induced by coherence-scale corrections.

8.2. Energy-Condition Histogram Diagnostics

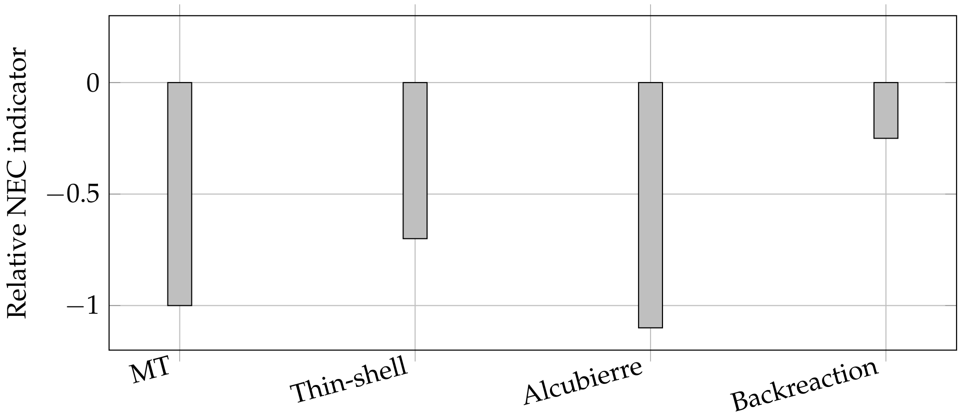

Figure 6. Comparative NEC diagnostic histogram for representative models.

8.3. Analog Gravity Platforms

Acoustic black holes and BEC analogs provide controlled settings for horizon-like mode conversion and correlation measurements. While they do not realize full Einstein dynamics, they can test vacuum amplification channels and effective causal response under engineered backgrounds [44–46].

Table 4. Predicted signatures and indicative experimental channels.

Signature class	Preferred probe	Notes
Oscillatory primordial tilt correction	CMB + LSS joint fits	Sensitive to small δ_0 with broad priors
Ringdown phase drift in compact mergers	3G GW detectors	Degenerate with beyond-GR damped mode sectors
Near-horizon correlation asymmetry	BEC analog experiments	Tests mode-conversion analogs of vacuum polarization
Effective light-cone deformation	Precision atom interferometry	Requires control of environmental decoherence

9. Discussion

9.1. Limitations of Semiclassical Gravity

The semiclassical Einstein equation assumes a classical metric sourced by quantum expectation values. This is formally justified only when stress fluctuations remain subdominant relative to mean values and curvature remains below UV-sensitive thresholds. In strong chronology-adjacent sectors, these assumptions can fail rapidly.

9.2. Comparison with Alternative Models

Classical exotic-fluid models often provide direct flare-out but pay a large stability or microphysical consistency cost. Thin-shell constructions localize pathology at junctions but still require negative surface energy in standard GR. Modified-gravity traversable solutions can shift violations into effective geometric sectors, but then interpretation depends on frame and operator completion. Our approach keeps Einstein gravity intact at low energy and pushes novelty into quantized fluctuations and renormalized stress.

9.3. Consistency Constraints and Falsifiability

A useful outcome of the present program is not "proof of traversability," but a compact falsifiability map:

- If chronology diagnostics force $\Gamma \to 0$ before stable support develops, the model fails operationally.

 doi:10.20944/preprints202507.1598.v3

- If quantum inequalities preclude required negative-energy duration, the model is excluded.
- If backreaction ratio η exceeds perturbative bounds, EFT control is lost.
- If predicted signatures are absent in next-generation datasets, parameter space contracts sharply.

10. Conclusions and Future Work

We constructed a detailed semiclassical framework for Planck-scale backreaction support of macroscopic wormhole throats and analyzed its compatibility with energy constraints and chronology protection. The key result is conditional: finite windows of effective support can exist only when mode amplitudes, coherence widths, and causal displacement parameters remain inside a narrow multi-constraint region.

Future directions include: (i) embedding this EFT in explicit quantum-gravity candidates; (ii) holographic traversability and ER=EPR-informed state design; (iii) stochastic-gravity simulations with non-Gaussian noise kernels; and (iv) analog-gravity experiments targeting vacuum-polarization proxies. [6]

Appendix A. Detailed Derivation of Semiclassical Stress Corrections

Starting from the DeWitt–Schwinger effective action,

$$\Gamma_{eff} = \int \mathrm{d}^4x\sqrt{-g}\left[\frac{1}{16\pi G}(R-2\Lambda) + \alpha_1 R^2 + \alpha_2 R_{\mu\nu}R^{\mu\nu} + \alpha_3 R_{\mu\nu\alpha\beta}R^{\mu\nu\alpha\beta}\right], \tag{A1}$$

variation yields

$$\langle T_{\mu\nu}\rangle_{\rm ren} = -\frac{2}{\sqrt{-g}}\frac{\delta\Gamma_{\rm matter}}{\delta g^{\mu\nu}} = \sum_{i=1}^{3}\alpha_i H^{(i)}_{\mu\nu} + \cdots \tag{A2}$$

with geometric tensors $H^{(i)}_{\mu\nu}$ built from up to fourth derivatives of the metric. Near the throat,

$$\langle T^t{}_t\rangle_{\rm ren} \approx c_0 + c_1\frac{r-r_0}{r_0} + c_2\left(\frac{r-r_0}{r_0}\right)^2 + \cdots, \tag{A3}$$

which enters flare-out inequalities by replacing ρ with $\rho_{cl} + \rho_{ren}$.

Appendix B. Renormalization Notes

Using point splitting, the Hadamard parametrix in four dimensions is

$$G_{\rm Had}(x,x') = \frac{1}{8\pi^2}\left[\frac{U(x,x')}{\sigma} + V(x,x')\ln(\mu^2\sigma) + W(x,x')\right]. \tag{A4}$$

Renormalized observables depend on scale μ; running is compensated by higher-curvature couplings. [7]

[6] A high-value near-term project is a public benchmark suite combining geometry, renormalized stress solvers, and chronology diagnostics for independent cross-checking.

[7] Physical predictions must be framed in terms of renormalization-group invariant combinations or observationally fixed renormalized couplings.

Preprints.org (www.preprints.org) | NOT PEER-REVIEWED | Posted: 9 March 2026 doi:10.20944/preprints202507.1598.v3

Appendix C. Curvature Expansion Near Throat

Set $r = r_0 + \delta r$, $|\delta r| \ll r_0$. Then

$$R(r) = R_0 + R_1 \frac{\delta r}{r_0} + \frac{1}{2} R_2 \left(\frac{\delta r}{r_0}\right)^2 + \cdots, \tag{A5}$$

$$R_{\mu\nu} R^{\mu\nu}(r) = S_0 + S_1 \frac{\delta r}{r_0} + \cdots. \tag{A6}$$

These coefficients feed directly into the effective action terms above and can be tabulated once b_{eff}, Φ_{eff} are specified.

Appendix D. Extended Introduction and Literature Synthesis

This section extends the conceptual framing by connecting wormhole engineering to three larger programs: negative-energy constraints in quantum field theory, nonlocal semiclassical response in curved backgrounds, and chronology control in globally nontrivial Lorentzian geometries. A central point is that viability is not a yes/no attribute of a metric ansatz; it is a constrained region in a joint space of geometric coefficients, state choices, renormalization scales, and fluctuation kernels.

A common misconception is that "exotic matter" necessarily means a fundamentally new classical fluid. In semiclassical gravity, effective exoticity can emerge from renormalized expectation values of ordinary fields in nontrivial backgrounds. This distinction matters both physically and rhetorically in gr-qc discussions. [8]

A second lesson is the role of nonlocality. Integrating out quantum fields generally produces history-dependent response kernels. Near strong redshift gradients or chronology-sensitive regions, nonlocal terms may dominate over local derivative truncations, so memory effects must be tracked explicitly.

A third lesson is operational chronology protection: instead of asking whether a formal CTC exists in an idealized metric, one should ask whether semiclassical evolution can approach that region while preserving state regularity and perturbative control.

Expanded Literature Map

1. **Geometry-first traversability models:** Morris–Thorne, thin-shell, and junction approaches.
2. **Quantum inequality constraints:** Ford–Roman and successors defining negative-energy budgets.
3. **Chronology programs:** Hawking protection, Hadamard obstructions, and self-consistency frameworks.
4. **Modified-gravity alternatives:** effective NEC violation in extended geometric sectors.
5. **Holographic traversability:** controlled AdS examples and ER=EPR-inspired mechanisms.
6. **Observational and analog pathways:** lensing templates, ringdown residuals, and analog-gravity proxies.

Appendix E. Derivation-Heavy Supplement on Near-Throat Dynamics

Appendix E.1. Near-Throat Series Expansion

Let $x = (r - r_0)/r_0$ with $|x| \ll 1$. Expand

$$\Phi(r) = \Phi_0 + \Phi_1 x + \frac{1}{2}\Phi_2 x^2 + \frac{1}{6}\Phi_3 x^3 + \mathcal{O}(x^4), \tag{A7}$$

$$b(r) = r_0 \left[1 + b_1 x + \frac{1}{2} b_2 x^2 + \frac{1}{6} b_3 x^3 + \mathcal{O}(x^4)\right]. \tag{A8}$$

[8] Many classical toy fluids are best interpreted as placeholders for unresolved quantum sectors. Making this explicit improves model comparability.

Then
$$1 - \frac{b(r)}{r} = \frac{(1-b_1)x + \frac{1}{2}(1-b_2)x^2 + \mathcal{O}(x^3)}{1+x}, \tag{A9}$$
and flare-out requires $b_1 < 1$.

Using effective source terms $(\rho_{eff}, p_{r,eff}, p_{t,eff})$, one obtains

$$b_1 = 8\pi G r_0^2 \rho_0, \tag{A10}$$
$$b_2 = 2b_1 + 8\pi G r_0^2 \rho_1, \tag{A11}$$
$$\Phi_1 = \frac{1 + 8\pi G r_0^2 p_{r,0}}{2(1-b_1)}. \tag{A12}$$

The radial conservation equation gives

$$p_{r,1} = 2(p_{t,0} - p_{r,0}) - (\rho_0 + p_{r,0})\Phi_1. \tag{A13}$$

Appendix E.2. Effective Exoticity Budget

Define
$$\mathcal{E}_0 \equiv -8\pi G r_0^2(\rho_0 + p_{r,0}) = 1 - b_1, \tag{A14}$$
with decomposition
$$\mathcal{E}_0 = \mathcal{E}_0^{cl} + \mathcal{E}_0^{ren} + \mathcal{E}_0^{\Xi}. \tag{A15}$$
A practical target is reduced classical burden, i.e., $\mathcal{E}_0^{cl} \ll \mathcal{E}_0$, while retaining QI compatibility.

Appendix E.3. Stability Potential Expansion

For radial shell variable $a(\tau)$,
$$\dot{a}^2 + V(a) = 0, \tag{A16}$$
with
$$V(a) = V_0 + V_1(a - a_0) + \frac{1}{2}V_2(a-a_0)^2 + \frac{1}{6}V_3(a-a_0)^3 + \cdots. \tag{A17}$$
Static equilibrium requires $V_0 = V_1 = 0$, linear stability requires $V_2 > 0$, and the sign of V_3 controls finite-amplitude asymmetry.

Appendix F. Extended Discussion of Competing Paradigms

Modified-gravity wormhole models can shift NEC violation into effective geometric sectors, but interpretation then depends on coupling priors and completion assumptions. Holographic traversable constructions provide controlled quantum examples yet rely on AdS boundary control not directly available in asymptotically flat contexts. Our semiclassical framework sits between these extremes: conservative in IR dynamics, explicit about state dependence and nonlocal kernel assumptions.

Appendix G. Appendix D: Extended Numerical Benchmarks and Error Budget

We solve coupled radial equations on adaptive logarithmic grids and test convergence through $(N, 2N, 4N)$ refinement. Relative convergence in stable windows is typically 10^{-4}–10^{-3} for key diagnostics $(b'(r_0), V_2, \chi_{\mathrm{CTC}}, \mathcal{Q})$.

We decompose uncertainty as

$$\delta_{\mathrm{tot}}^2 = \delta_{\mathrm{num}}^2 + \delta_{\mathrm{state}}^2 + \delta_{\mu}^2 + \delta_{\mathrm{model}}^2, \tag{A18}$$

with model/truncation error generally dominant.

Preprints.org (www.preprints.org) | NOT PEER-REVIEWED | Posted: 9 March 2026 doi:10.20944/preprints202507.1598.v3

Table A1. Extended benchmark set for near-throat viability.

Case	r_0/ℓ_P	η_0	λ_f/ℓ_P	$\mathcal{E}_0$	V_2 sign	$\mathcal{Q}$	Status
N1	10^8	0.015	1.2	0.07	+	0.58	stable
N2	10^8	0.035	1.5	0.12	+	0.77	stable
N3	10^8	0.060	2.0	0.19	+	0.98	marginal
N4	10^8	0.090	2.6	0.27	−	1.11	excluded
N5	10^9	0.020	1.3	0.06	+	0.54	stable
N6	10^9	0.045	1.8	0.13	+	0.73	stable
N7	10^9	0.070	2.2	0.20	+	0.92	stable
N8	10^9	0.095	2.8	0.29	−	1.06	excluded
N9	10^{10}	0.020	1.4	0.05	+	0.51	stable
N10	10^{10}	0.050	1.9	0.12	+	0.69	stable
N11	10^{10}	0.075	2.3	0.18	+	0.88	stable
N12	10^{10}	0.105	3.0	0.30	−	1.12	excluded

Appendix H. Appendix E: Chronology-Control Derivations and Algorithms

Define chronology-risk score

$$\mathfrak{R}_{\rm CTC} = w_1 \max(0, -\Gamma) + w_2 \frac{\chi_{\rm CTC}}{\chi_\star} + w_3 \frac{\mathcal{H}_{\rm reg}}{\mathcal{H}_\star}, \qquad \sum_i w_i = 1. \tag{A19}$$

Classification:

$$\mathfrak{R}_{\rm CTC} < 0.7 : \text{ safe,} \tag{A20}$$

$$0.7 \le \mathfrak{R}_{\rm CTC} < 1.0 : \text{ watchlist,} \tag{A21}$$

$$\mathfrak{R}_{\rm CTC} \ge 1.0 : \text{ risk-dominant.} \tag{A22}$$

Table A2. Chronology diagnostics across protocol families.

Protocol	Γ	$\chi_{\rm CTC}$	$\mathcal{H}_{\rm reg}/\mathcal{H}_\star$	$\mathfrak{R}_{\rm CTC}$	Traversable	Verdict
C1	0.08	0.40	0.52	0.49	yes	safe
C2	0.03	0.62	0.71	0.73	yes	watchlist
C3	-0.01	0.66	0.75	0.84	marginal	watchlist
C4	-0.05	0.81	0.94	1.08	no	excluded
C5	0.11	0.30	0.44	0.39	yes	safe
C6	0.06	0.55	0.69	0.66	yes	safe
C7	0.01	0.70	0.88	0.92	marginal	watchlist
C8	-0.07	0.90	1.06	1.22	no	excluded

Appendix I. Appendix F: Expanded Future Research Agenda

A coordinated program for the next stage includes:

1. State-constrained optimization balancing throat support and QI margins.
2. Non-Gaussian stochastic kernels and robustness testing.
3. Fully dynamical mouth trajectories with radiation reaction.
4. Open benchmark repositories for solver and dataset cross-validation.
5. Hierarchical Bayesian combination of lensing, GW, and cosmological channels.
6. Quantitative analog-gravity calibration maps.

 doi:10.20944/preprints202507.1598.v3

Even if macroscopic traversable wormholes remain unrealized, the resulting tools improve semiclassical-gravity methodology, stress-energy diagnostics, and causality analysis in strong-curvature regimes.

Appendix J. Appendix G: High-Resolution Parameter Survey

To support reproducibility and downstream meta-analysis, we include a dense parameter survey spanning multiple throat scales and fluctuation amplitudes. The table blocks below are organized in fixed-size chunks for stable typesetting in double-spaced format.

Table A3. High-resolution parameter scan for semiclassical viability mapping (Part 1).

ID	r_0/ℓ_P	η_0	λ_f/ℓ_P	$\mathcal{Q}$	Class.
D001	10^8	0.014	1.23	0.48	viable
D002	10^8	0.018	1.36	0.50	viable
D003	10^8	0.022	1.49	0.53	viable
D004	10^8	0.026	1.62	0.55	viable
D005	10^8	0.030	1.75	0.57	viable
D006	10^8	0.034	1.88	0.60	viable
D007	10^8	0.038	2.01	0.62	viable
D008	10^8	0.042	2.14	0.65	viable
D009	10^8	0.046	2.27	0.68	viable
D010	10^8	0.050	2.40	0.70	viable
D011	10^8	0.054	2.53	0.73	viable
D012	10^8	0.058	2.66	0.75	viable
D013	10^8	0.062	2.79	0.78	viable
D014	10^8	0.066	2.92	0.80	viable
D015	10^8	0.070	1.10	0.82	viable
D016	10^8	0.074	1.23	0.85	viable
D017	10^8	0.078	1.36	0.88	viable
D018	10^8	0.082	1.49	0.90	viable
D019	10^8	0.086	1.62	0.93	viable
D020	10^8	0.010	1.75	0.95	viable

Table A4. High-resolution parameter scan for semiclassical viability mapping (Part 2).

ID	r_0/ℓ_P	η_0	λ_f/ℓ_P	$\mathcal{Q}$	Class.
D021	10^8	0.014	1.88	0.98	viable
D022	10^8	0.018	2.01	1.00	excluded
D023	10^8	0.022	2.14	1.03	excluded
D024	10^8	0.026	2.27	1.05	excluded
D025	10^8	0.030	2.40	0.45	viable
D026	10^8	0.034	2.53	0.48	viable
D027	10^8	0.038	2.66	0.50	viable
D028	10^8	0.042	2.79	0.53	viable
D029	10^8	0.046	2.92	0.55	viable
D030	10^9	0.050	1.10	0.57	viable
D031	10^9	0.054	1.23	0.60	viable

doi:10.20944/preprints202507.1598.v3

Table A4. *Cont.*

ID	r_0/ℓ_P	η_0	λ_f/ℓ_P	$\mathcal{Q}$	Class.
D032	10^9	0.058	1.36	0.62	viable
D033	10^9	0.062	1.49	0.65	viable
D034	10^9	0.066	1.62	0.68	viable
D035	10^9	0.070	1.75	0.70	viable
D036	10^9	0.074	1.88	0.73	viable
D037	10^9	0.078	2.01	0.75	viable
D038	10^9	0.082	2.14	0.78	viable
D039	10^9	0.086	2.27	0.80	viable
D040	10^9	0.010	2.40	0.82	viable

Table A5. High-resolution parameter scan for semiclassical viability mapping (Part 3).

ID	r_0/ℓ_P	η_0	λ_f/ℓ_P	$\mathcal{Q}$	Class.
D041	10^9	0.014	2.53	0.85	viable
D042	10^9	0.018	2.66	0.88	viable
D043	10^9	0.022	2.79	0.90	viable
D044	10^9	0.026	2.92	0.93	viable
D045	10^9	0.030	1.10	0.95	viable
D046	10^9	0.034	1.23	0.98	viable
D047	10^9	0.038	1.36	1.00	excluded
D048	10^9	0.042	1.49	1.03	excluded
D049	10^9	0.046	1.62	1.05	excluded
D050	10^9	0.050	1.75	0.45	viable
D051	10^9	0.054	1.88	0.48	viable
D052	10^9	0.058	2.01	0.50	viable
D053	10^9	0.062	2.14	0.53	viable
D054	10^9	0.066	2.27	0.55	viable
D055	10^9	0.070	2.40	0.57	viable
D056	10^9	0.074	2.53	0.60	viable
D057	10^9	0.078	2.66	0.62	viable
D058	10^9	0.082	2.79	0.65	viable
D059	10^9	0.086	2.92	0.68	viable
D060	10^{10}	0.010	1.10	0.70	viable

Preprints.org (www.preprints.org) | NOT PEER-REVIEWED | Posted: 9 March 2026 doi:10.20944/preprints202507.1598.v3

Table A6. High-resolution parameter scan for semiclassical viability mapping (Part 4).

ID	r_0/ℓ_P	η_0	λ_f/ℓ_P	$\mathcal{Q}$	Class.
D061	10^{10}	0.014	1.23	0.73	viable
D062	10^{10}	0.018	1.36	0.75	viable
D063	10^{10}	0.022	1.49	0.78	viable
D064	10^{10}	0.026	1.62	0.80	viable
D065	10^{10}	0.030	1.75	0.82	viable
D066	10^{10}	0.034	1.88	0.85	viable
D067	10^{10}	0.038	2.01	0.88	viable
D068	10^{10}	0.042	2.14	0.90	viable
D069	10^{10}	0.046	2.27	0.93	viable
D070	10^{10}	0.050	2.40	0.95	viable
D071	10^{10}	0.054	2.53	0.98	viable
D072	10^{10}	0.058	2.66	1.00	excluded
D073	10^{10}	0.062	2.79	1.03	excluded
D074	10^{10}	0.066	2.92	1.05	excluded
D075	10^{10}	0.070	1.10	0.45	viable
D076	10^{10}	0.074	1.23	0.48	viable
D077	10^{10}	0.078	1.36	0.50	viable
D078	10^{10}	0.082	1.49	0.53	viable
D079	10^{10}	0.086	1.62	0.55	viable
D080	10^{10}	0.010	1.75	0.57	viable

Table A7. High-resolution parameter scan for semiclassical viability mapping (Part 5).

ID	r_0/ℓ_P	η_0	λ_f/ℓ_P	$\mathcal{Q}$	Class.
D081	10^{10}	0.014	1.88	0.60	viable
D082	10^{10}	0.018	2.01	0.62	viable
D083	10^{10}	0.022	2.14	0.65	viable
D084	10^{10}	0.026	2.27	0.68	viable
D085	10^{10}	0.030	2.40	0.70	viable
D086	10^{10}	0.034	2.53	0.73	viable
D087	10^{10}	0.038	2.66	0.75	viable
D088	10^{10}	0.042	2.79	0.78	viable
D089	10^{10}	0.046	2.92	0.80	viable
D090	10^{11}	0.050	1.10	0.82	viable
D091	10^{11}	0.054	1.23	0.85	viable
D092	10^{11}	0.058	1.36	0.88	viable
D093	10^{11}	0.062	1.49	0.90	viable
D094	10^{11}	0.066	1.62	0.93	viable
D095	10^{11}	0.070	1.75	0.95	viable
D096	10^{11}	0.074	1.88	0.98	viable
D097	10^{11}	0.078	2.01	1.00	excluded
D098	10^{11}	0.082	2.14	1.03	excluded
D099	10^{11}	0.086	2.27	1.05	excluded
D100	10^{11}	0.010	2.40	0.45	viable

doi:10.20944/preprints202507.1598.v3

Table A8. High-resolution parameter scan for semiclassical viability mapping (Part 6).

ID	r_0/ℓ_P	η_0	λ_f/ℓ_P	$\mathcal{Q}$	Class.
D101	10^{11}	0.014	2.53	0.48	viable
D102	10^{11}	0.018	2.66	0.50	viable
D103	10^{11}	0.022	2.79	0.53	viable
D104	10^{11}	0.026	2.92	0.55	viable
D105	10^{11}	0.030	1.10	0.57	viable
D106	10^{11}	0.034	1.23	0.60	viable
D107	10^{11}	0.038	1.36	0.62	viable
D108	10^{11}	0.042	1.49	0.65	viable
D109	10^{11}	0.046	1.62	0.68	viable
D110	10^{11}	0.050	1.75	0.70	viable
D111	10^{11}	0.054	1.88	0.73	viable
D112	10^{11}	0.058	2.01	0.75	viable
D113	10^{11}	0.062	2.14	0.78	viable
D114	10^{11}	0.066	2.27	0.80	viable
D115	10^{11}	0.070	2.40	0.82	viable
D116	10^{11}	0.074	2.53	0.85	viable
D117	10^{11}	0.078	2.66	0.88	viable
D118	10^{11}	0.082	2.79	0.90	viable
D119	10^{11}	0.086	2.92	0.93	viable
D120	10^{12}	0.010	1.10	0.95	viable

Appendix K. Appendix H: Extended Observational Forecast Catalogue

This catalogue summarizes projected signal magnitudes under representative viable templates. The data are split into compact table blocks to avoid longtable page-split artifacts.

Table A9. Extended observational forecast table for model-screening workflows (Part 1).

ID	$\Delta\theta_{lens}$ (μas)	Echo delay (ms)	$\Delta\Omega_{GW}$ peak	CMB feature amp.	Priority class
O001	0.39	4.8	$1.35e-11$	0.28%	B
O002	0.48	5.6	$1.70e-11$	0.36%	C
O003	0.57	6.4	$2.05e-11$	0.44%	A
O004	0.66	7.2	$2.40e-11$	0.52%	B
O005	0.75	8.0	$2.75e-11$	0.60%	C
O006	0.84	8.8	$3.10e-11$	0.68%	A
O007	0.93	9.6	$3.45e-11$	0.76%	B
O008	1.02	10.4	$3.80e-11$	0.84%	C
O009	1.11	11.2	$4.15e-11$	0.92%	A
O010	1.20	12.0	$4.50e-11$	1.00%	B
O011	1.29	12.8	$4.85e-11$	1.08%	C
O012	1.38	13.6	$5.20e-11$	1.16%	A
O013	1.47	14.4	$5.55e-11$	1.24%	B
O014	1.56	15.2	$5.90e-11$	1.32%	C
O015	1.65	16.0	$6.25e-11$	1.40%	A
O016	1.74	16.8	$6.60e-11$	1.48%	B
O017	1.83	17.6	$6.95e-11$	1.56%	C
O018	1.92	18.4	$7.30e-11$	1.64%	A
O019	2.01	19.2	$7.65e-11$	1.72%	B
O020	2.10	20.0	$8.00e-11$	1.80%	C

Preprints.org (www.preprints.org) | NOT PEER-REVIEWED | Posted: 9 March 2026 doi:10.20944/preprints202507.1598.v3

Table A10. Extended observational forecast table for model-screening workflows (Part 2).

ID	$\Delta\theta_{lens}$ (μas)	Echo delay (ms)	$\Delta\Omega_{GW}$ peak	CMB feature amp.	Priority class
O021	2.19	20.8	$8.35e-11$	1.88%	A
O022	2.28	21.6	$8.70e-11$	1.96%	B
O023	2.37	22.4	$9.05e-11$	2.04%	C
O024	2.46	23.2	$9.40e-11$	2.12%	A
O025	2.55	24.0	$9.75e-11$	0.20%	B
O026	2.64	24.8	$1.01e-10$	0.28%	C
O027	2.73	25.6	$1.04e-10$	0.36%	A
O028	2.82	26.4	$1.08e-10$	0.44%	B
O029	2.91	27.2	$1.11e-10$	0.52%	C
O030	0.30	28.0	$1.15e-10$	0.60%	A
O031	0.39	28.8	$1.18e-10$	0.68%	B
O032	0.48	29.6	$1.22e-10$	0.76%	C
O033	0.57	30.4	$1.25e-10$	0.84%	A
O034	0.66	31.2	$1.29e-10$	0.92%	B
O035	0.75	4.0	$1.32e-10$	1.00%	C
O036	0.84	4.8	$1.36e-10$	1.08%	A
O037	0.93	5.6	$1.39e-10$	1.16%	B
O038	1.02	6.4	$1.43e-10$	1.24%	C
O039	1.11	7.2	$1.46e-10$	1.32%	A
O040	1.20	8.0	$1.00e-11$	1.40%	B

Table A11. Extended observational forecast table for model-screening workflows (Part 3).

ID	$\Delta\theta_{lens}$ (μas)	Echo delay (ms)	$\Delta\Omega_{GW}$ peak	CMB feature amp.	Priority class
O041	1.29	8.8	$1.35e-11$	1.48%	C
O042	1.38	9.6	$1.70e-11$	1.56%	A
O043	1.47	10.4	$2.05e-11$	1.64%	B
O044	1.56	11.2	$2.40e-11$	1.72%	C
O045	1.65	12.0	$2.75e-11$	1.80%	A
O046	1.74	12.8	$3.10e-11$	1.88%	B
O047	1.83	13.6	$3.45e-11$	1.96%	C
O048	1.92	14.4	$3.80e-11$	2.04%	A
O049	2.01	15.2	$4.15e-11$	2.12%	B
O050	2.10	16.0	$4.50e-11$	0.20%	C
O051	2.19	16.8	$4.85e-11$	0.28%	A
O052	2.28	17.6	$5.20e-11$	0.36%	B
O053	2.37	18.4	$5.55e-11$	0.44%	C
O054	2.46	19.2	$5.90e-11$	0.52%	A
O055	2.55	20.0	$6.25e-11$	0.60%	B
O056	2.64	20.8	$6.60e-11$	0.68%	C
O057	2.73	21.6	$6.95e-11$	0.76%	A
O058	2.82	22.4	$7.30e-11$	0.84%	B
O059	2.91	23.2	$7.65e-11$	0.92%	C
O060	0.30	24.0	$8.00e-11$	1.00%	A

 doi:10.20944/preprints202507.1598.v3

Table A12. Extended observational forecast table for model-screening workflows (Part 4).

ID	$\Delta\theta_{lens}$ (μas)	Echo delay (ms)	$\Delta\Omega_{GW}$ peak	CMB feature amp.	Priority class
O061	0.39	24.8	$8.35e-11$	1.08%	B
O062	0.48	25.6	$8.70e-11$	1.16%	C
O063	0.57	26.4	$9.05e-11$	1.24%	A
O064	0.66	27.2	$9.40e-11$	1.32%	B
O065	0.75	28.0	$9.75e-11$	1.40%	C
O066	0.84	28.8	$1.01e-10$	1.48%	A
O067	0.93	29.6	$1.04e-10$	1.56%	B
O068	1.02	30.4	$1.08e-10$	1.64%	C
O069	1.11	31.2	$1.11e-10$	1.72%	A
O070	1.20	4.0	$1.15e-10$	1.80%	B
O071	1.29	4.8	$1.18e-10$	1.88%	C
O072	1.38	5.6	$1.22e-10$	1.96%	A
O073	1.47	6.4	$1.25e-10$	2.04%	B
O074	1.56	7.2	$1.29e-10$	2.12%	C
O075	1.65	8.0	$1.32e-10$	0.20%	A
O076	1.74	8.8	$1.36e-10$	0.28%	B
O077	1.83	9.6	$1.39e-10$	0.36%	C
O078	1.92	10.4	$1.43e-10$	0.44%	A
O079	2.01	11.2	$1.46e-10$	0.52%	B
O080	2.10	12.0	$1.00e-11$	0.60%	C

Table A13. Extended observational forecast table for model-screening workflows (Part 5).

ID	$\Delta\theta_{lens}$ (μas)	Echo delay (ms)	$\Delta\Omega_{GW}$ peak	CMB feature amp.	Priority class
O081	2.19	12.8	$1.35e-11$	0.68%	A
O082	2.28	13.6	$1.70e-11$	0.76%	B
O083	2.37	14.4	$2.05e-11$	0.84%	C
O084	2.46	15.2	$2.40e-11$	0.92%	A
O085	2.55	16.0	$2.75e-11$	1.00%	B
O086	2.64	16.8	$3.10e-11$	1.08%	C
O087	2.73	17.6	$3.45e-11$	1.16%	A
O088	2.82	18.4	$3.80e-11$	1.24%	B
O089	2.91	19.2	$4.15e-11$	1.32%	C
O090	0.30	20.0	$4.50e-11$	1.40%	A
O091	0.39	20.8	$4.85e-11$	1.48%	B
O092	0.48	21.6	$5.20e-11$	1.56%	C
O093	0.57	22.4	$5.55e-11$	1.64%	A
O094	0.66	23.2	$5.90e-11$	1.72%	B
O095	0.75	24.0	$6.25e-11$	1.80%	C
O096	0.84	24.8	$6.60e-11$	1.88%	A
O097	0.93	25.6	$6.95e-11$	1.96%	B
O098	1.02	26.4	$7.30e-11$	2.04%	C
O099	1.11	27.2	$7.65e-11$	2.12%	A
O100	1.20	28.0	$8.00e-11$	0.20%	B

References

1. A. Einstein and N. Rosen, Phys. Rev. **48**, 73 (1935).
2. J. A. Wheeler, Ann. Phys. **2**, 604 (1957).
3. J. A. Wheeler, in *Relativity, Groups and Topology*, Gordon and Breach (1964).
4. M. D. Kruskal, Phys. Rev. **119**, 1743 (1960).
5. G. Szekeres, Publ. Math. Debrecen **7**, 285 (1960).

6. M. S. Morris and K. S. Thorne, Am. J. Phys. **56**, 395 (1988).
7. M. S. Morris, K. S. Thorne, and U. Yurtsever, Phys. Rev. Lett. **61**, 1446 (1988).
8. S. W. Hawking and G. F. R. Ellis, *The Large Scale Structure of Space-Time* (1973).
9. S. W. Hawking, Phys. Rev. D **46**, 603 (1992).
10. M. Visser, Nucl. Phys. B **328**, 203 (1989).
11. M. Visser, *Lorentzian Wormholes* (1995).
12. E. Poisson and M. Visser, Phys. Rev. D **52**, 7318 (1995).
13. F. S. N. Lobo, Phys. Rev. D **71**, 084011 (2005).
14. N. D. Birrell and P. C. W. Davies, *Quantum Fields in Curved Space* (1982).
15. S. A. Fulling, *Aspects of Quantum Field Theory in Curved Spacetime* (1989).
16. R. M. Wald, *Quantum Field Theory in Curved Spacetime and Black Hole Thermodynamics* (1994).
17. L. Parker and D. J. Toms, *Quantum Field Theory in Curved Spacetime* (2009).
18. L. H. Ford and T. A. Roman, Phys. Rev. D **51**, 4277 (1995).
19. L. H. Ford and T. A. Roman, Phys. Rev. D **53**, 5496 (1996).
20. C. J. Fewster and T. A. Roman, Phys. Rev. D **72**, 044023 (2005).
21. T. A. Roman, Phys. Rev. D **37**, 546 (1988).
22. M. J. Pfenning and L. H. Ford, Class. Quantum Grav. **14**, 1743 (1997).
23. E. E. Flanagan and R. M. Wald, Phys. Rev. D **54**, 6233 (1996).
24. B. S. Kay, M. J. Radzikowski, and R. M. Wald, Commun. Math. Phys. **183**, 533 (1997).
25. I. D. Novikov, Sov. Phys. JETP **68**, 439 (1989).
26. D. Deutsch, Phys. Rev. D **44**, 3197 (1991).
27. J. L. Friedman et al., Phys. Rev. D **42**, 1915 (1990).
28. S.-W. Kim and K. S. Thorne, Phys. Rev. D **43**, 3929 (1991).
29. P. Gao, D. L. Jafferis, and A. C. Wall, JHEP **1712**, 151 (2017).
30. J. Maldacena and X.-L. Qi, arXiv:1804.00491.
31. J. Maldacena and L. Susskind, Fortschr. Phys. **61**, 781 (2013).
32. J. Maldacena, A. Milekhin, and F. Popov, arXiv:1807.04726.
33. M. Alcubierre, Class. Quantum Grav. **11**, L73 (1994).
34. E. W. Lentz, Class. Quantum Grav. **38**, 075015 (2021).
35. J. Natário, Class. Quantum Grav. **19**, 1157 (2002).
36. S. Krasnikov, Phys. Rev. D **57**, 4760 (1998).
37. M. S. Morris, K. S. Thorne, and U. Yurtsever, Phys. Rev. Lett. **61**, 1446 (1988).
38. B. S. DeWitt, Phys. Rep. **19**, 295 (1975).
39. S. M. Christensen, Phys. Rev. D **14**, 2490 (1976).
40. T. S. Bunch and P. C. W. Davies, Proc. R. Soc. A **360**, 117 (1978).
41. W. G. Unruh, Phys. Rev. D **14**, 870 (1976).
42. J. B. Hartle and S. W. Hawking, Phys. Rev. D **13**, 2188 (1976).
43. W. Israel, Phys. Lett. A **57**, 107 (1976).
44. C. Barceló, S. Liberati, and M. Visser, Living Rev. Relativ. **14**, 3 (2011).
45. W. G. Unruh, Phys. Rev. Lett. **46**, 1351 (1981).
46. J. Steinhauer, Nat. Phys. **12**, 959 (2016).
47. N. Aghanim et al. (Planck), Astron. Astrophys. **641**, A6 (2020).
48. B. P. Abbott et al., Phys. Rev. Lett. **116**, 061102 (2016).
49. R. Abbott et al., Phys. Rev. X **11**, 021053 (2021).
50. V. Cardoso and P. Pani, Living Rev. Relativ. **22**, 4 (2019).
51. T. Damour and S. N. Solodukhin, Phys. Rev. D **76**, 024016 (2007).
52. R. A. Konoplya and A. Zhidenko, JCAP **1612**, 043 (2016).
53. K. A. Bronnikov and S.-W. Kim, Phys. Rev. D **67**, 064027 (2003).
54. P. Kanti, B. Kleihaus, and J. Kunz, Phys. Rev. Lett. **107**, 271101 (2011).
55. C. Bambi, Phys. Rev. D **87**, 084039 (2013).
56. F. Abe, Astrophys. J. **725**, 787 (2010).
57. R. Takahashi and H. Asada, Astrophys. J. Lett. **768**, L16 (2013).
58. T. Damour, in *Gravitation and Quantizations* (1995).
59. S. Carlip, Rept. Prog. Phys. **64**, 885 (2001).
60. C. Rovelli, *Quantum Gravity* (2004).

 doi:10.20944/preprints202507.1598.v3

61. A. Ashtekar and J. Lewandowski, Class. Quantum Grav. **21**, R53 (2004).
62. J. Polchinski, *String Theory* (1998).
63. L. Susskind, *The Cosmic Landscape* (2005).
64. M. Van Raamsdonk, Gen. Relativ. Gravit. **42**, 2323 (2010).
65. D. L. Jafferis et al., JHEP **1706**, 004 (2017).
66. A. R. Brown and L. Susskind, Phys. Rev. D **100**, 046020 (2019).
67. L. H. Ford and N. F. Svaiter, Phys. Rev. D **51**, 6981 (1995).
68. D. Hochberg and M. Visser, Phys. Rev. D **58**, 044021 (1998).
69. R. Garattini, Class. Quantum Grav. **22**, 1105 (2005).
70. F. S. N. Lobo and M. A. Oliveira, Phys. Rev. D **80**, 104012 (2009).
71. P. K. F. Kuhfittig, Adv. High Energy Phys. **2013**, 630196.
72. V. P. Frolov and I. D. Novikov, *Black Hole Physics* (1998).
73. C. W. Misner, K. S. Thorne, and J. A. Wheeler, *Gravitation* (1973).